ELSEVIER

Journal of Nuclear Materials 241–243 (1997) 444–449

journal of nuclear materials

Deduction of SOL transport coefficients using 2D modelling for hot-ion ELM-free H-modes in JET

G.K. McCormick [a,b,*], A. Chankin [a], S. Clement [a], S. Davies [a], J. Ehrenberg [a], A. Loarte [a], R. Monk [a], R. Simonini [a], J. Spence [a], M. Stamp [a], A. Taroni [a], G. Vlases [a]

[a] *JET Joint Undertaking, OX14 3EA Abingdon, Oxfordshire, UK*

[b] *Max-Planck-Institut für Plasmaphysik, Boltzmannstr. 2, 85748 Garching, Germany*

Abstract

Profiles of T_e and J_{sat} measured by Langmuir probes at the target plates of the JET MkI divertor and the target plate power loading are modelled via the EDGE2D/NIMBUS codes. The low-density ($\bar{n}_e \sim 1 \times 10^{19}$ m^{-3}) OH plasma preceding high-power NBI, as well as the ELM-free high performance H* and high performance rollover H^{RO} phases are considered. Experimentally, the power splitting between ions ($P_i \geq 7$ MW) and electrons ($P_e < 1$ MW) in conjunction with the H-mode transport barrier effects that T_e and J_{sat} change little from OH to H* conditions, although $P_{in} \sim 2 \rightarrow 20$ MW and $\bar{n}_e$ can increase up to a factor of three as the H*-phase progresses. In modelling, χ_i is taken as 1 m^2/s. To match the divertor T_e-profiles, χ_e must be varied from the strike point outwards as $\sim 0.5 \rightarrow 3$ m^2/s in all phases. Perpendicular particle transport is assumed to be purely diffusive or with a pinch. Duplication of $J_{sat}(R)$ requires: $D_\perp \sim 0.03 \rightarrow 0.015$ m^2/s (OH $\rightarrow$ H*), or $v_{pinch}/D_\perp \sim 15 \rightarrow 45 \rightarrow 25$ m^{-1} (OH $\rightarrow$ H* $\rightarrow$ H^{RO}) with $D_\perp = 0.1$ m^2/s. Sensitivity studies involving different recycling scenarios, deep and shallow computational grids, wall material and the thermal transport barrier are carried out to judge the possible influences on the deduced transport coefficients.

Keywords: JET; SOL plasma; Tokamak; 2D model; Transverse transport

1. Introduction

The ELM-free hot-ion H-mode is the mainstay of the JET D-T campaign and, in addition, represents an extreme corner of low-recycling SOL/divertor operational/modelling space. A marked difference in accessibility to this regime existed between the single null up (SNU) dump-plate configuration of 1991–1992 and the MkI divertor of 1994–1995: Whereas ELMs on SNU were an exception, type I ELMy H-modes were a natural feature of MkI. Only through dedicated experiments leading to minimal recycling conditions as well as optimization of triangularity and edge shear could a satisfactory ELM-free situation be recovered [1].

On JET the duration of the ELM-free period appears dictated by the approach of the edge pressure gradient to ballooning or kink instability limits [2]. The rate of formation of this gradient seems correlated with the level of recycling and thus implicitly with the nature of plasma–wall interaction and shielding efficiency of the edge/SOL plasma against recycling neutrals. Since attainment and protraction of the ELM-free period is vital for the success of JET D-T operation and generally for VH-modes and because analysis of the ELM-free situation can provide insights as to the nature of those processes leading to the breakdown of the edge transport barrier via an ELM or outer mode [1], this study is intended to establish a baseline for continuing code/machine-based investigations on control of these events.

2. Temporal behaviour and power accountability

In Fig. 1 the temporal development of a hot-ion H-mode is considered, this particular shot being chosen because of

* Corresponding author. Tel.: +44-1235 464 972; fax: +44-1235 464 766; e-mail: gmccor@jet.uk.

PII S0022-3115(96)00544-2

the availability of divertor diagnostics and sudden turn-on of the event leading to a rollover in the D–D reaction rate R_{DD}: An X-point is formed at 11.5 s leading to a pronounced decrease in $\bar{n}_e$ when the diverted OH plasma makes target plate contact. Neutral injection heating of $P_{NBI} \sim 17.5$ MW is initiated at 12 s where $\bar{n}_e$ ($\sim 1 \times 10^{19}$ m^{-3}) is such that shine-through is moderate ($\sim 30\%$). $\bar{n}_e$ then climbs at a rate 30–40% in excess of beam fuelling (with no gas puff), i.e. there is a wall source of neutrals. Important to note is that neither the divertor D_α, saturation current J_{sat} to a target plate Langmuir probe or the subdivertor neutral pressure P_{SD} undergo significant changes from the OH phase. At 12.96 s an outer mode [1] provokes a temporal rollover both in R_{DD} and diamagnetic energy W_{dia}, leading to a prompt augmentation of flux to the target as registered in the D_α signal. In the pre-rollover phase $P_{loss} = P_{abs} + P_{OH} - dW_{dia}/dt - P_{rad} \sim 10$ MW. At the rollover, P_{loss} increases to ~ 16 MW. Using a simple 1D heat transport model for the plates, the rapid rise in target plate temperature indicates an approximate power loading of $P_{out}^{target} \geq 8$ MW and $P_{in}^{target} \geq 3$ MW at the outer and inner divertor target plates respectively. In discharges where the increase in RDD is limited by a giant ELM rather than a rollover there is generally not a large change in divertor signals or power to the targets before the ELM.

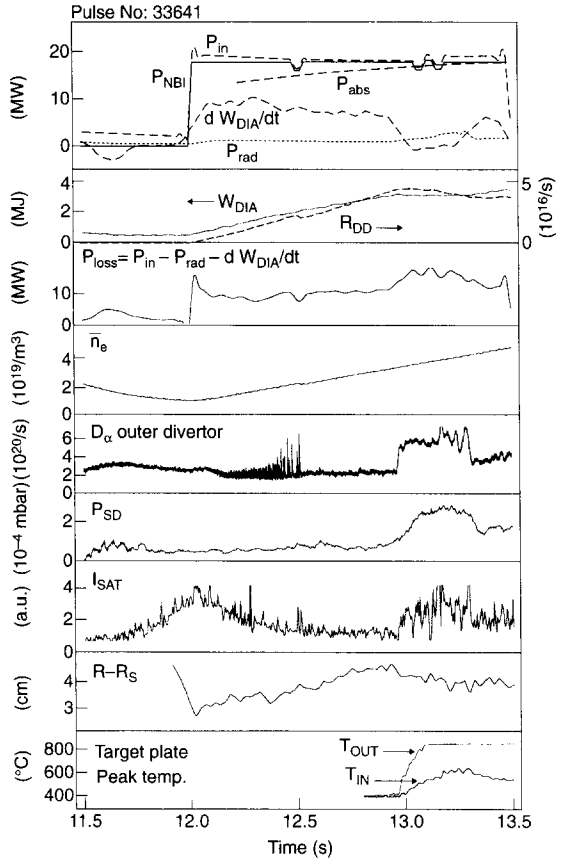

Fig. 1. Time traces for global (top four boxes) and divertor parameters. $\bar{n}_e$ = line-averaged density; D_α gives the photons/s emanating from the entire outer target plate.

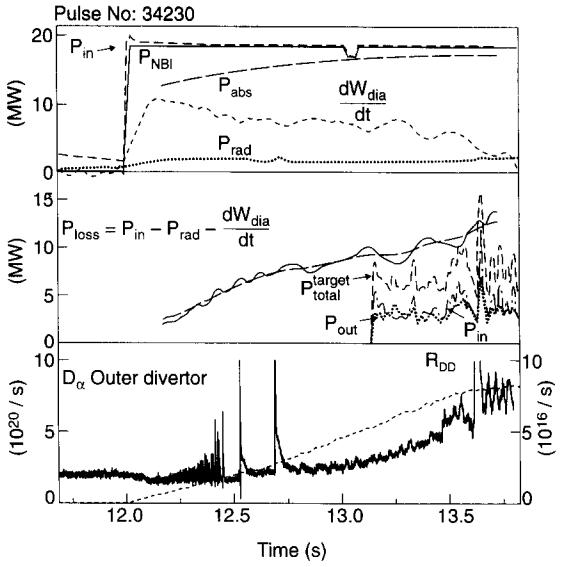

Fig. 2. #34230, $P_{in} = P_{NBI} + P_{OH}$; P_{abs} = absorbed NBI power (calculated); $P_{loss} = P_{abs} + P_{OH} - dW_{dia}/dt - P_{rad}$ (the dashed line gives the time-averaged value). Inner and outer target plate power loading deduced from IR camera measurements in conjunction with a 3D heat transport algorithm. D_α (photons/s) from the entire outer target plate.

For code calculations the sum of electron and ion power, $P_{SOL} = P_e + P_i$, at the innermost computational grid boundary must be consistent with the power to the target plates estimated from P_{loss} and with P_{total}^{target} estimated from IR camera measurements. Due to the short ELM-free period (< 1.3 s) and technical aspects, few hot-ion H-mode discharges exist where IR camera measurements yield target plate power fluxes. In #34230 of Fig. 2 one finds $P_{in}^{target} \sim P_{out}^{target}$, such that $P_{total}^{target} \sim 6$ MW in the ELM-free phase and 9.5 MW at the rollover. Thus, on average, $P_{loss} - P_{total}^{target} \sim 2.8$–$4.5$ MW for H^* and ~ 1.5 MW for H^{RO}. (This latter number will actually be larger as W_{dia} does not resolve the short rollover phase.) Another discharge (#34236) with $P_{loss} \sim 7.5$ MW yields $P_{in}^{target} \sim P_{out}^{target} \sim 3$ MW, giving $P_{loss} - P_{total}^{target} \sim 1.5$ MW for H^*. Hence, for these two examples the deficit between P_{loss} and P_{total}^{target} ranges over 1.5–4.5 MW, not taking into account uncertainties involved in P_{NBI} (± 1 MW), P_{OH} (from neoclassical resistivity), P_{abs} (± 0.5 MW), P_{total}^{target} (± 1 MW) and dW_{dia}/dt. Since part of this deficit may originate from charge-exchange (CX) core losses not encompassed by the grid, $P_{SOL} \sim 7$ MW (H^*) and ~ 12 MW (H^{RO}) are used in modelling shot #32919 – for which IR data does not exist, but which has a P_{loss} of magnitude close to #34230–#34236.

3. EDGE2D setup and exploratory investigations

The ultimate goals of this study, χ_e and $D_\perp$, are inferred by reproducing the outer target plate experimental profiles of J_{sat} and T_e via code calculations. Some details of the code setup as well as the sensitivity of χ_e and $D_\perp$ to various code scenarios are discussed in Sections 3.1 and 3.2.

3.1. Sensitivity studies

More than 40 EDGE2D/NIMBUS runs have been performed to arrive at best fits for J_{sat} and T_{ed}, using $D_\perp$ alone or with a pinch, for three phases (OH, H* and H^{RO}) of #32919. This shot was chosen as: (a) it is the best HFE shot, (b) acceptable target plate Langmuir probe data is available and (c) core parameters are excellently documented. The effects of different recycling scenarios, $P_e - P_i$ power splitting, thermal transport barrier, deep versus shallow grids have been explored in order to judge consequences on derived transport coefficients and other experimentally-relevant code outputs.

The divertor substructure, including cryopump and bypasses to the main chamber are included, with the pumped neutrals being reintroduced into the main chamber as a uniform puff. Only one equilibrium grid is used to model the three phases, with a spatial extent of -0.4 or -9.5 cm (deep core) to $+1.8$ cm around the separatrix at the outer midplane. Diffusion alone, or with a pinch is assumed in modelling, constant on flux surfaces. Drifts are not considered. The upstream midplane density at the outer separatrix n_{es} as well as P_e and P_i are specified as inputs. A limit for ion momentum flux along field lines is employed [3]. $Z_{eff} = 1$ is assumed. $Z_{eff} \geq 2$ is more accurate ($Z_{eff} \leq 1.5$ in the core), which would lead to lower T_{ed} in the calculations. But then a full multi-fluid treatment needs be implemented — and this would have been too CPU time intensive for these studies. It is estimated that $> 50\%$ of the typically 1 MW of radiation in a hot-ion mode originates from Cu and Ni [4] and the rest from carbon.

Detailed modelling uses a recycling coefficient $R = 1$ with walls and target of CFC, i.e. a steady-state situation. Using the deep core (whose radial $\overline{n_e L}$ to the inner grid boundary was adjusted to roughly represent the experimental transport barrier), the particle flux passing through the inner grid boundary was allowed to accumulate at a rate 5×10^{20} s^{-1}, consistent with experiment. This loss was accommodated by either allowing $R > 1$ or introducing an inner wall puff – both options being possible explanations for the excess fuelling observed. The resultant computed profiles of J_{sat} and T_{ed} suffered only minor variations from the static case; thus, assuming $R = 1$ should have little impact on deduced values of $D_\perp$ and χ_e.

About 2/3 of the main chamber walls facing the plasma consist of inconel. One deep-core run with all-iron walls was performed to test the effect of deep-fuelling expected from the higher particle and energy reflection coefficients associated with metals: The SOL/divertor profiles changed little, but n_e at the inner grid increased by 25% while n_{es} was held constant – implying if enhanced core fuelling is an important aspect of exacerbating pressure-gradient-driven modes, then one may expect metallic walls to degrade high performance discharges and probably H-mode quality in general. The topics of core neutral density, its relationship to metallic walls and potential effects on H-mode properties have been discussed elsewhere [5].

If a radially constant χ_e is used in deep core calculations, equipartition is so strong between electrons and ions that the upstream (midplane) T_{es} is always too large to be consistent with experimental downstream (divertor) T_{ed}, no matter what P_e is chosen within the relationship $P_e + P_i = 7$ MW. By allowing χ_e to vary spatially from smaller to larger values ($0.1 \rightarrow 0.4$ m^2/s, for example) from the inner core to the separatrix — thus augmenting the core temperature gradient — it is possible to depress T_{es} to a more reasonable level and bring the predicted core T_e closer to experiment. Clearly, if an expanded core region is under scrutiny — with the H-mode in particular — it is necessary to fully model the transport barrier as well as the SOL in order to make relevant statements. Since a sharp H-mode-like transport barrier is presently not implemented within EDGE2D, all calculations were done with the shallow core.

3.2. Other considerations

χ_e is forced to vary as $A + B/n_e$ to better fit T_{ed} profiles at the target plate. A and B are adjusted such that about the same χ_e profile results (~ 0.5–3 m^2/s from the strike point outwards) regardless of n_{es}. χ_i is held constant at 1 m^2/s, for lack of better information.

Upstream parameters are not available for any hot-ion H-mode shots on MkI. Prior to MkI, for the H-mode $\lambda_{ne}^{SOL} \sim 1^+$ cm (exponential density falloff length at the outer midplane). Similar discharges on MkI show $\lambda_{ne}^{SOL} \sim 1^+$ cm is of the order 1 cm [6]. It transpires that when modelling particle transport with a pinch, the J_{sat} profile can be credibly fitted by adjusting $v_{pinch}/D_\perp$ and $D_\perp$ may be selected to match λ_{ne}^{SOL}. For these studies $D_\perp = 0.1$ m^2/s was chosen, yielding $\lambda_{ne}^{SOL} \sim 0.85$ cm for the H* phase when $v_{pinch}/D_\perp = 45$. This freedom to match upstream λ_{ne}^{SOL} and downstream $\lambda_{J_{sat}}^{div}$ (target plate J_{sat} falloff length) does not exist using diffusion alone.

4. EDGE2D/NIMBUS modelling of #32919

Referring to Fig. 3, Langmuir probe profiles are modelled for the time slices: 51.75–52.0 s (OH), 52.55–52.9 s (H*) and 53.1–53.2 s (H^{RO}). Table 1 lists the code input parameters. Salient code and experimental results are sum-

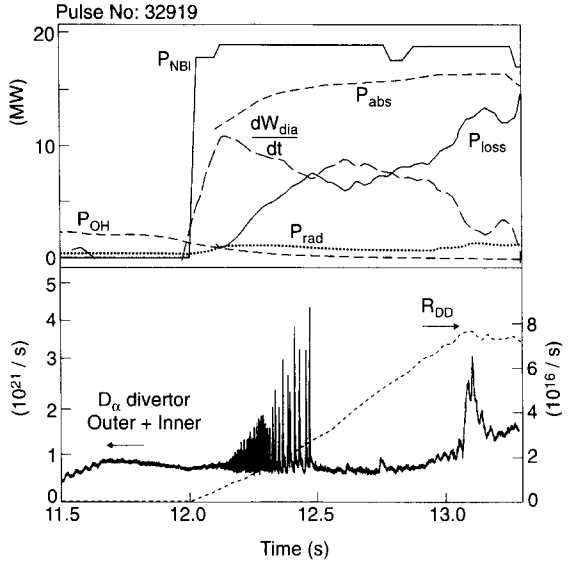

Fig. 3. Global parameters for shot #32919.

marized in Table 2. Aside from OH where $P_e = P_i$ is taken, P_e is selected ($P_e \ll P_i$) to approximately reproduce T_{ed} – use of a realistic Z_{eff} will bring the codes absolute T_{ed} values still closer to experiment. Half (estimated from experiment) of P_{rad} is radiated within the grid via a global carbon radiation function.

Code-experiment profile comparisons are shown in Figs. 4–6. Inner-plate comparisons are not considered as the experimental profiles are not well-defined. We discuss

Table 1
Summary of code input parameters for Fig. 4Fig. 5Fig. 6

	OH		H*		H^RO
	diff.	pinch	diff.	pinch	pinch
P_e (MW)	0.9	0.9	0.1	0.4	0.5
P_i (MW)	0.9	0.9	7	7	12
P_{RAD} (MW)	0.2	0.2	0.5	0.5	0.8
n_{es} (10^{19} m^{-3})	0.6	0.55	0.7	0.5	0.85
$D_\perp$ (m^2/s)	0.03	0.1	0.015	0.1	0.1
$v_{pinch}/D_\perp$ (m^{-1})	–	15	–	45	25
χ_e (m^2/s)	0.5–2		0.7–3		0.5–3
χ_i (m^2/s)	1.0		1.0		1.0

upstream density behaviour first: For OH, essentially the same $n_{es} \sim 0.55$–0.6×10^{19} m^{-3} is required for both pure diffusion (PD) and the pinch to duplicate J_{sat}^{peak}, whereas for H*(PD) $n_{es} \sim 0.7 \times 10^{19}$ m^{-3} versus 0.5×10^{19} m^{-3} for H*(pinch). Even though J_{sat}^{peak} and n_{es} change little over OH → H*, the divertor density $n_{ed,out}^{peak}$ drops a factor of two, this being related to $T_{id} \gg T_{ed}$ in the H*-phase. A marked difference in predicted upstream profiles is found: λ_{ne}^{SOL}(PD, H*) ~ 0.5 cm, which at a distance of 7 mm from the separatrix then flattens to ~ 2.5 cm. In contrast, λ_{ne}^{SOL}(pinch, H*) ~ 0.84 cm. In experiment, λ_{sat}^{div} (OH → H*) varies as 5.6 → 4 cm. To reproduce this, transport needs be changed as: $D_\perp = 0.03 \rightarrow 0.015$ m^2/s (PD) or $v_{pinch}/D_\perp = 15 \rightarrow 45$ (pinch). The $\lambda_{J_{sat}}^{div}$ (H*) profiles computed using pure diffusion tend to turn unrealistically upwards at the outer edge of the grid. In contrast, pure

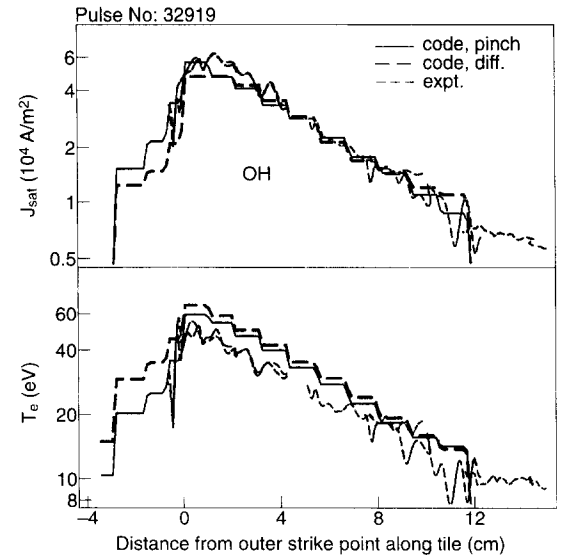

Fig. 4. Comparison of experimental J_{sat} and T_e-profiles at the outer target plate for the *OH phase* (51.75–52.0 sec) and the modelled results using diffusion alone, or with a pinch. The salient code input values are summarized in Table 1.

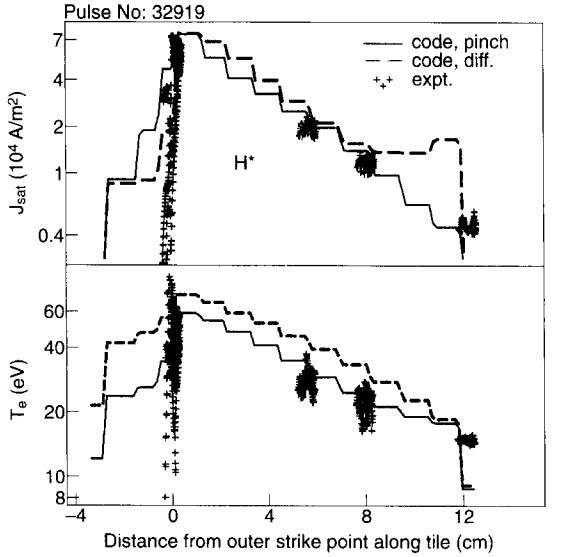

Fig. 5. Comparison of experimental J_{sat} and T_e-profiles at the outer target plate for the *high performance phase*, H^* (52.55–52.9 s) and the modelled results using diffusion alone, or with a pinch. The salient code input values are summarized in Table 1.

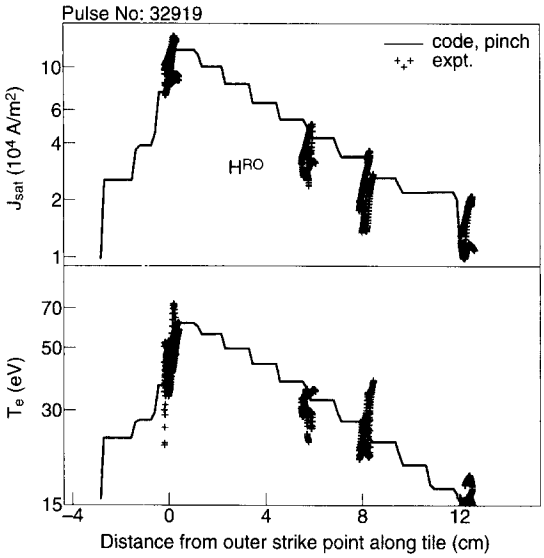

Fig. 6. Comparison of experimental J_{sat} and T_e-profiles at the outer target plate for the *rollover phase* H^{RO} (53.1–53.2 s) and the modelled results using diffusion with a pinch. The salient code input values are summarized in Table 1.

diffusion better fits the private flux region, perhaps indicating that different transport laws are needed to describe different regions.

The rollover phase is modelled in an average sense by increasing $v_{pinch}/D_\perp$ to 25 and n_{es} to 0.85×10^{19} m^{-3}. $P_{SOL} = P_e + P_i = 12.5$ MW is used to bring P_{total}^{target} (total power to target plates) into line with shots #33641 or #34230 of Figs. 1 and 2. From Table 2 we note as P_{SOL} increases (OH $\rightarrow$ H* $\rightarrow$ H^{RO}), the calculations predict both CX neutrals and equipartition with electrons — P_{CX} and $P_{i\rightarrow e}$ respectively — to become more important loss channels for ion power.

Electron temperature profiles are broad in all three phases. The fits shown in Figs. 4–6 are achieved using an option available within the code ($\chi_e = A + B/n_e$) as described in Section 3.2. Other analysis also suggests χ_e changes spatially in this fashion [7]. The poorer agreement between experiment and code in the private flux region is an artefact of using the n_e^{-1} scaling and is not of importance for this work.With respect to other quantities, the computed $P_{SD} \sim 4 \times 10^{-5}$ mbar during H* is typical of hot-ion H-modes. In Table 2 the code D_α (in/out) at the target plates agree with experiment during OH, but are too

Table 2
Summary of code and experimental values

		OH		H*		H^{RO}	
		in	out	in	out	in	out
J_{sat}^{peak} (A/cm^2)	expt.	?	6.3	10	7.4	~ 9–15	9–16
	code	7.1	5.8	7.8	7.7	12.6	12.3
$\lambda_{J_{sat}}^{div}$ (cm)	expt.	?	5.5	?	4.2	?	5.5
	code	7.8	5.6	5.8	4.0	7.1	5.3
$T_{e,div}^{peak}$ (eV)	expt.	?	55	35	~ 50	33	~ 50
	code	54	62	56	60	56	61
$\lambda_{T_e}^{div}$ (cm)	expt.	?	7.5	?	10	?	~ 10
	code	8.5	6.7	12	8	11.4	8.2
$T_{i,div}^{peak}$ (eV)	code	44	61	655	661	571	560
$n_{e,div}^{peak}$ (10^{19} m^{-3})	code	0.64	0.48	0.27	0.26	0.46	0.46
n_{es} (out. midp.) (10^{19} m^{-3})	diff.		0.6		0.7		–
	pinch		0.55		0.5		~ 0.85
$\lambda_{ne,SOL}$ (cm)	diff.		1.1		0.53 $\rightarrow$ 2.5 at 7 mm		
	pinch		1.43		0.84		1.26
P_{in-out}^{target} (MW)	code	0.59	0.74	2.44	2.94	4.1	5.0
$P_{i\rightarrow e}$ (MW)	code		0.12		0.85		1.88
P_{CX} (MW)	code		0.18 (60%)		1.4 (70%)		2.4 (77%)
ϕ_{targ} (10^{22} s^{-1})	code	1.34	1.3	1.0	1.2	2.1	2.5
Total D_α (10^{20} s^{-1})	expt.	4.5	3.6	4.7	3.0	10–17	7–14
	code	4.8	3.9	2.2	2.4	5.5	5.7
Horiz. D_α (10^{18} m^{-2} s^{-1})	expt.		1.68		1.86		2.3–2.8
	code		0.56		0.47		0.95

'code' = code calculation with pinch; 'diff' = code calculation with pure diffusion. 'peak' refers to peak values at the target plates. 'div' denotes target plate values. The subscripts 'e, i' denote electron and ion values respectively. 'ϕ_{targ}' is the ion flux to the target plates. D_α is in units of photons/s. Other quantities are defined in the text.

low in the H-mode phase by 20–50%, even for the outer plate whose J_{sat} profile is reasonably modelled. D_α from molecules is not included in the code estimate, which will make up part of the difference. D_α^{horiz} arises from a horizontal viewing chord near the midplane which faces into the inner inconel wall. The code value is 30–50% of experiment. Code experience is that using metallic walls will increase D_α^{horiz} by 50% and use of the deep core by another $\sim 50\%$, so agreement with experiment is acceptable.

5. Summary

Using EDGE2D/NIMBUS, the outer target J_{sat} and T_{ed} profiles and measured power to the plates have been modelled for the ELM-free and rollover phases, as well as the NBI-target OH plasma, of a low-recycling high performance discharge. These profiles undergo minor changes in passing from OH – to H*-conditions, the difference being in power to the plate via the ions. Little NBI power is transmitted to the electron SOL, i.e. $P_i \gg P_e$ and $T_{id} \gg T_{ed}$. The H-mode transport barrier serves to isolate the divertor from dynamic activity of core where $\bar{n}_e$ can increase a factor of three during the ELM-free period with virtually no change in upstream density or particle flux to the target plate. (Invariance of the SOL density profile during the H* phase has also been documented on ASDEX [8].) The rollover phase is modelled via an increase in perpendicular particle transport above H*, about a factor of two increase in n_{es} and augmentation in P_{SOL} of perhaps 50%.

On JET an inwards pinch has been found useful in duplicating SOL parameters under high recycling conditions [9]. In the results presented here, pure diffusion produces distorted profiles in the far SOL under H* conditions, because $D_\perp$ is very small. (Allowing $D_\perp$ to vary spatially may ameliorate this effect.) Use of a pinch permits larger $D_\perp$, as long as $v_{pinch}/D_\perp$ is adjusted correctly, resulting in predicted profiles fairly resilient against recycling levels – which is observed experimentally in the hot-ion H-mode. Although $D_\perp$ 0.1 m^2/s (in conjunction with a pinch) seems in accord with circumstantial experimental evidence, combined upstream–downstream measurements with the MkII divertor are necessary to make a convincing case for the absolute value of $D_\perp$, or for one form of transport or another.

$v_{pinch}/D_\perp = 15$ is a common value for L-mode plasmas [9]. $D_\perp = 0.03$ m^2/s is lower than $D_\perp \sim 0.05$ m^2/s (using $D_\perp$ constant on flux surfaces) [10] found for higher-density OH conditions. $\chi_e \sim \chi_i \sim 1$ m^2/s is typical of L-mode, but here $\lambda_{T_e}^{target}$ actually increases for OH → H*, necessitating $\chi_e(H^*, H^{RO}) > \chi_e(OH)$. This result is not sensitive to the exact value of χ_i.

The ratio $P_i/P_e > 10$ (Table 1) does not reflect the power splitting of the core, but that outside the transport barrier. Inclusion of the main plasma — in accord with the transport barrier — in a self-consistent manner with experimental parameters at the target plates is now being undertaken by combining the core transport code JETTO with EDGE2D/NIMBUS [11]. This will enable power splitting to be addressed as well as estimate volume CX power losses not covered by the 'thin-core' model used here. Out of 19 MW injected, there is (on average) a difference of 3–4 MW (H*) between $P_{loss} = P_{abs} + P_{OH} - dW_{dia}/dt - P_{rad}$ and P_{total}^{target} (from the IR camera). Present calculations can account for $P_{CX} = 1.4$ MW via CX neutrals – 70% occurring below the X-point (This percentage is delineated by parenthesis in Table 2.) – with P_{CX} being almost independent of n_{es}. Hence, even without inclusion of CX losses from the core, power accountability is reasonable.

Acknowledgements

The authors gratefully acknowledge discussions and support from P. Andrew, A. Bickley, J. Christiansen, P. Coad, T.C.C. Jones, R. König, P. Lomas, D. Muir and R. Reichle.

References

[1] T.C.C. Jones et al., Plasma Phys. Contr. Fusion 37 (1995) A359.
[2] G.T.A. Huysmans et al., Proc. 22nd EPS Conf. Bournemouth 19C (1995) I-201.
[3] G. Radford, Contrib. Plasma Phys. 32 (1992) 297.
[4] K. Lawson, JET Joint Undertaking, private communication.
[5] K. Itoh and S.-I. Itoh, Plasma Phys. Control. Fusion 37 (1995) 491.
[6] D.D.R. Summers et al., these Proceedings, p. 391.
[7] S.K. Erents et al., these Proceedings, p. 433.
[8] G.K. McCormick, Z.A. Pietrzyk et al., J. Nucl. Mater. 162–164 (1989) 264.
[9] A. Taroni et al., Proc. 22nd EPS Conf. Bournemouth 19C (1995) IV-297.
[10] A. Loarte et al., Proc. 22nd EPS Conf. Bournemouth 19C (1995) III-305.
[11] A. Taroni et al., in: Proc. 23rd EPS Conf. Kiew (1996) to be published.